DFT Investigation of Alkoxide Formation from Olefins in H-ZSM-5

Aditya Bhan, Yogesh V. Joshi, W. Nicholas Delgass, and Kendall T. Thomson*

School of Chemical Engineering, Purdue University, West Lafayette, Indiana 47907

Received: February 13, 2003; In Final Form: July 2, 2003

We present a density functional theory (DFT) study of propene, 1-hexene, and 3-hexene protonation over representative H-ZSM-5 clusters to give covalent alkoxide intermediates. The influence of cluster size, olefin carbon number, olefin conformation, proton siting, aluminum siting, and bonding configuration (primary vs secondary) of the alkoxide intermediate was analyzed. We found the formation of a physisorbed π-complex involving the olefin double bond and the acidic proton to be relatively independent of olefin structure and site geometry. However, we show that the proton-transfer process for formation of the covalent alkoxide intermediate involves a carbenium-ion-like transition state, with an activation energy that is (1) dependent on the protonation site of the olefin and (2) relatively independent of the carbon number and double bond location of the olefin. Accessibility of the alkoxide oxygen site in the cavity was observed to play a significant role in the stability of the alkoxy species. We find that the overall energy of adsorption for alkoxides depends strongly on the crystallographic Al site and the specific host oxygen for the Brønsted proton. For larger alkenes we find a dependence on alkoxide conformations and report a 5 kcal/mol difference in energies of formation for different rotational orientations of 3-hexene alkoxide intermediates. Finally, we report a novel reaction path for propene chemisorption, whereby the primary alkoxide is bonded to the Brønsted host oxygen rather than a neighboring oxygen.

1. Introduction

A fundamental component of zeolite catalytic activity is Brønsted acidity. The unique environment of Brønsted acid sites in the micropores of zeolites contributes greatly to their reactivity as contrasted by the relatively weak acidity of amorphous aluminosilicates. In pursuit of a fundamental understanding of Brønsted acidity, computational methods have emerged as a powerful tool, and a great deal of work has been performed in the past decade to model catalytically actives sites in zeolites using the quantum mechanical cluster approach.[1−6] In particular, one can obtain information pertinent to the local electronic and structural properties of the zeolite as well as the potential energy surface characterizing interactions with guest molecules. In this context, quantum chemical calculations have been of great utility and allowed researchers to analyze the structure, nature, and relative stability of reaction intermediates and transition states for catalytic reactions that cannot be directly studied experimentally.[1−4,6−12]

In this work we apply electronic density functional theory (DFT) to study olefin adsorption in H-ZSM-5. Paraffin adsorption in zeolites has been well studied experimentally.[13−19] However, for unsaturated olefinic molecules, interaction with Brønsted acid sites often results in oligomerization,[20,21] and hence experimental measurements for adsorption energetics represent a challenge. In situ spectroscopic studies (solid-state NMR and IR) of the interaction of Brønsted acid sites with adsorbed molecules have demonstrated that carbenium ions are not stable within zeolite cavities and that protonation of adsorbed olefins and alcohols results in the formation of covalent alkoxide species.[21−23] In consonance with these experimental observations, several quantum chemical studies also conclude that the protonation of olefins by Brønsted acid sites results in formation of covalently bonded alkoxide species and that carbenium-ion-like species exist only as transition states through which reactions of these species proceed.[1,5,6,24] Theoretical studies[1,6,24,25] have also highlighted the role of the neighboring negatively charged oxygen atoms of the oxide surface, which play the role of basic sites. Consequently, it is believed that olefin chemisorption involves, in a concerted manner, (1) the proton transfer from the Brønsted site onto a carbon atom of the olefin double bond and (2) the simultaneous C−O bond formation at the adjacent oxygen of the zeolite structure.

Although the basic concepts of olefin protonation in zeolites have been studied by quantum mechanical calculations at different levels of theory, there are still questions concerning the bifunctional (acid−base) mechanism, formation, stability, and activation barrier of the alkoxide intermediate. In addition, due to the small cluster size typically used for these calculations, the protonation of large alkenes has also not been addressed.

In this work we investigate the protonation mechanisms of olefins in H-ZSM-5, at the DFT level of theory, with representative cluster sizes (up to 25 Si/Al atoms per cluster) to gain insights into the relative stability of alkoxy species and the barriers and mechanism for their formation from olefins as well as the interaction of saturated paraffin molecules with Brønsted acid sites. We investigated the interaction of propane, propene, 1-hexene, and 3-hexene with H-ZSM-5 by means of cluster calculations and report associated interaction energies of the corresponding physisorbed π-complexes and the adsorption energies of the respective alkoxy species on representative ZSM-5 clusters. Transition states associated with alkoxide formation were also computed to highlight the carbon number and isomer dependence of activation energies for alkoxide formation.

The remainder of this paper is organized as follows: In section 2 we provide details concerning the computational meth-

* To whom correspondence should be addressed. Phone: +1 765-496-6706. Fax: +1 765-494-0805. E-mail: thomsonk@ecn.purdue.edu.

10.1021/jp034382h CCC: $25.00
Published on Web 09/03/2003

odology and cluster selection. In section 3.1, we detail the effects of relaxation upon Al substitution in the ZSM-5 lattice. We describe the covalent interactions within the zeolite and also examine the effect of cluster size on relaxation. In section 3.2 we address the interaction of propene with the Brønsted acid site to form a physisorbed π-complex. In section 3.3, we describe the formation of the covalent alkoxide intermediate formed upon chemisorption of the propene molecule and discuss the effects of cluster size and termination on the chemisorption energy. Section 3.4 discusses the effect of carbon number and location of the olefinic double bond for formation of the physisorbed π-complex and chemisorbed alkoxide intermediate as we examine the interaction of 1-hexene and 3-hexene with the Brønsted acid site. In section 3.5, we describe the interaction of propane with the Brønsted acid site and compare our results with reported experimental values. Section 4 discusses the mechanistic and kinetic implications of our results, and in section 5 we offer conclusions from our work.

2. Computational Methodology

Geometry optimization calculations for minimum energy and transition-state structures were performed using nonlocal, gradient-corrected density functional theory (DFT). Zygmunt et al.[26] have assessed various density functional methods for studying molecular adsorption in zeolites. They conclude that the B3LYP functional gives intermolecular geometries and intermolecular vibrational frequencies similar to those obtained using MP2 and that B3LYP is the best choice for DFT treatment of molecular adsorption in zeolite systems. Hence, the B3LYP hybrid functional,[27] which includes a mixture of Hartree−Fock exchange with DFT exchange-correlation, was used for all calculations. Basis sets at the 6-31g(d) level (i.e., double-ζ level) with polarization functions added to all the atoms were used, with the exception of terminal and Brønsted acid hydrogens where polarization functions were excluded. No basis-set superposition error (BSSE) or zero-point energy (ZPE) corrections were considered in this work. Transition states were located by employing the quadratic synchronous transit (QST) algorithm[28] with the midpoint along the linear synchronous transit (LST) path being used as an initial guess for the QST optimization. All calculations were performed using GAUSSIAN 98.[29]

Cluster Selection. The cluster approach in DFT methods has contributed significantly to understanding olefin protonation in zeolites.[24,30,31] Until recently, most theoretical studies of zeolite-catalyzed reactions employed a small cluster of atoms (typically $HO(H)-Al(OH)_3$, $SiX_3-OH-AlX_2-OSiX_3$, with X = H, OH) to represent the Brønsted acid site. Moreover, the clusters used to model the active site often are not structurally distinguishable among particular zeolites and therefore are unable to explain the different catalytic attributes exhibited by structurally different zeolites. Further, recent theoretical studies have shown that there is a strong correlation between the local framework structure of the zeolite and the stability of the adsorbed surface intermediates.[7,32,33] To address these issues, more recent studies use either (i) large clusters,[34] (ii) combined quantum mechanics/molecular mechanics (QM/MM),[35,36] or (iii) periodic density functional calculations using plane waves as basis sets.[37−39] For these reasons, we opted to design representative clusters that were large enough to capture pertinent local features of specific zeolite sites.

ZSM-5 is a medium pore, high-silica zeolite with two-dimensional interconnected 10-ring channel system that exhibits valuable shape selective characteristics. For the purpose of this work we shall refer to ZSM-5 clusters as **nT** clusters depending on the number of tetrahedral Si or Al atoms incorporated in the cluster. Cluster size effects were considered by comparing **10T** and **25T** clusters with aluminum substitution at the T12 site (shown in Figure 1). Effects of different T-site locations were considered by comparing a **10T** cluster with aluminum substitution at the T12 site to a **15T** cluster with aluminum substitution at the T4 site. The **10T** cluster was terminated with Si−H and O−H bonds, while the **25T** and **15T** clusters were terminated with Si−H bonds. The terminal Si−H bond length was fixed at 1.498 Å along the direction of the silicon−oxygen bond as determined from crystallographic data.[40] To allow for site relaxation upon aluminum substitution, only the terminal hydrogens were fixed for the **10T** cluster, while for the **25T** and **15T** clusters the terminal silicon and hydrogen atoms were fixed at crystallographic locations. Additional geometric details about the optimized geometries are provided in section 3.

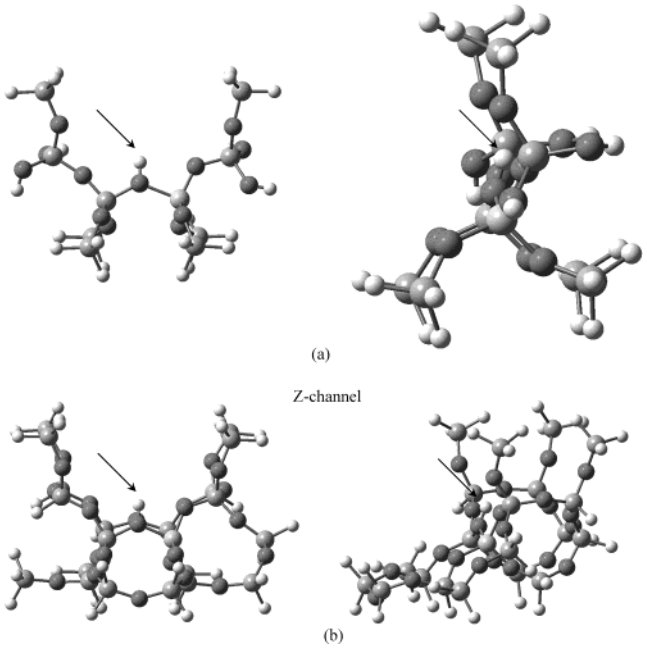

Figure 1. Structures of 10T and 25T clusters with aluminum substitution at the T12 site used for DFT calculations. The arrow indicates the location of the acidic proton.

3. Results

3.1. Cluster Relaxation. Figure 1 depicts the **10T** and **25T** clusters with Al substitution at the T12 site. Cluster size effects have been shown to be significant for deprotonation[41,42] and protolytic cracking[34] energetics, and therefore we investigated geometries at these two cluster sizes to examine and minimize effects of cluster size.

The results of our structural relaxation are presented in Table 1. The acidic proton was observed to reside 0.97 Å from the bridging oxygen, and the O−H distance was not observed to vary appreciably with cluster size. The Al−O−Si angle of 131.16° for the **25T** cluster decreased slightly in the **10T** cluster (130.20°). The O−T−O bond angle and the O−O distance were both observed to decrease upon Al substitution (88.6° versus 93.9°; 2.48 Å versus 2.69 Å in the **10T** cluster). Our calculations also predict that the Brønsted acid proton lies out of the plane of the Si−O−Al plane by 22.7 degrees, and a feature to note is the elongated Al−O bond length ($\Delta \sim 0.14$ Å) for the oxygen atom on which the Brønsted acid proton resides. The geometric

TABLE 1: Results of Structural Relaxation upon Al Substitution at the T12 Site[a]

structural parameter	10T Si cluster	10T Al cluster	25T Al cluster
r(T12−O)	1.64	1.94	1.84
r(O−H)		0.97	0.97
r(T12−H)		2.45	2.35
∠T12−O−T12	135.78	130.19	131.16
∠T12−O−H		110.04	109.02
∠O−T12−O	109.46	93.9	88.63
O Mulliken charge	−0.596	−0.730	−0.698
T Mulliken charge	1.200	0.952	0.882
H Mulliken charge		0.483	0.495

[a] Distances are in Å. Angles are in degrees.

data reported here are in general agreement with previous computational work concerning H-ZSM-5.[42,43]

The T−O bond length was observed to increase significantly upon Al substitution, consistent with the notion of a weaker Al−O bond strength. A signature of covalent bonding in these clusters is the shortening of the Si−O bond lengths that neighbor the Al-containing tetrahedron.[7] Our calculation predicts a decrease from 1.62 Å in silicalite to 1.59 Å in the Al-substituted **25T** cluster.

3.2. Propene Physisorption. Next we studied the interaction of the Brønsted acid site with propene resulting in a physisorbed π-complex. The **10T** cluster with the acidic proton residing on the O24 lattice oxygen was used. The relaxed physisorbed complex is shown in Figure 2(a).

The hydrogen atom of the OH group is attracted to the center of the propene double bond, and we observed the equilibrium position of the proton to be almost equidistant from the primary and secondary carbon atoms (2.10 and 2.26 Å respectively) in the relaxed physisorbed complex. Compared to unadsorbed propene, there was practically no difference in the geometry of the propene molecule in the physisorbed state. The C═C and C−C bond lengths, and the CCC bond angle, were observed to be nearly equal in both molecules. The charge on the terminal C1 carbon (−0.411e), however, differed significantly for propene within the zeolite cavity compared to the gas-phase molecule (−0.333e). The altered electronic environment of molecules within the zeolite cavity has also been observed by Corma and co-workers,[44−46] who attribute the enhanced reactivity of ethylene as well as the enhanced paraselectivity for electrophilic reactions of toluene in zeolites to this spatial confinement affect.

The physisorbed complex also has the observed effect of slightly elongating the O−H bond (0.99 Å, compared to the propene-free cluster O−H bond length of 0.97 Å). We calculated the frequency red shift of this interaction to be ≈530 cm $^{-1}$, which compares favorably with measured experimental values (539 cm^{-1})[47] for propene physisorption. All other geometric rearrangements were minor. The formation of the physisorbed π-complex was observed to be exothermic, and the calculated adsorption energy (total energy relative to the isolated cluster and propene molecule) was 8.8 kcal/mol.

3.3. Propene Alkoxide Formation. The formation of a secondary alkoxide from the physisorbed intermediate takes place through the calculated transition state shown in Figure 2(b). The geometry and electronic structure of the transition state for this reaction closely resemble the classical 2-propyl secondary carbenium ion. Comparing the transition state to the physisorbed state, we observed a lengthening of the C1−C2 bond from 1.333 Å (C═C double bond in the physisorbed state) to 1.456 Å (a value intermediate between C−C single and C═C double bonds). The O−H bond distance also increased significantly (to 1.97 Å), and the observed C1−H bond distance was 1.11 Å, which closely resembles the C1−H distance in the gas-phase propene molecule (1.088 Å). This leads us to postulate that the primary reaction coordinate in this reaction is the bonding of the C2 carbon to the neighboring basic oxygen (O20) site. Moreover, we observe hydrogen bonding interactions between the methyl group and the framework oxygen atoms at the transition-state geometry—see Figure 2(b)—similar to those observed by Correa et al.[33] for the protonation of butene isomers.

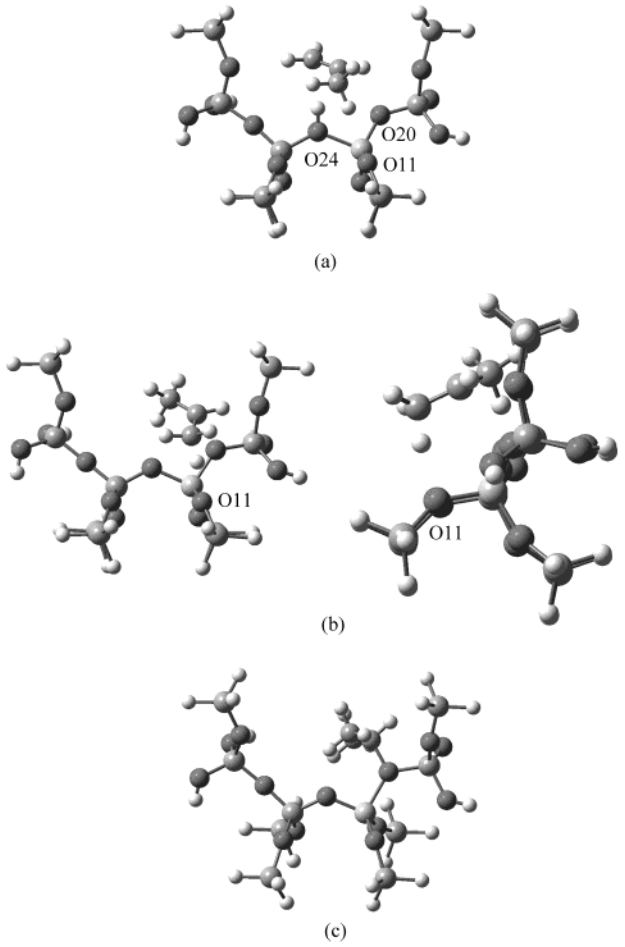

Figure 2. Optimized geometries for (a) π-complex, (b) transition state, and (c) alkoxide species formed during propene interaction with the Brønsted acid site located at O24 for the 10T cluster. Side and front views for the transition-state geometry are shown.

Relative to the physisorbed geometry, only minor changes in the Si−O−Al and O−Al−O bond angles were observed. A notable feature of the transition-state geometry is that as the proton detaches from the Brønsted acid site, the Al−O bond relaxes, resulting in identical Al−O bond lengths of 1.77 Å, compared to 1.93 Å (Al−O24) and 1.73 Å (Al−O20) for the physisorbed geometry. A Mulliken charge analysis reveals that the $C_3H_7^+$ transition state has high carbocation character, having a net charge of 0.695e. We computed the activation energy to be 18.6 kcal/mol (see Figure 3).

The resulting alkoxide complex for the C2−O20 bond is shown in Figure 2(c). The geometry of the C2 carbon in the alkoxide complex resembles that of a tetrahedrally coordinated carbon, and the 1.52 Å C2−O20 bond distance is similar to that observed in alcohols and other carbon−oxygen containing compounds. The C1−C2 and C2−C3 bond lengths are similar to those of single bonded C−C species in the gas phase. Another interesting geometric feature is the lengthening of the Al−O20

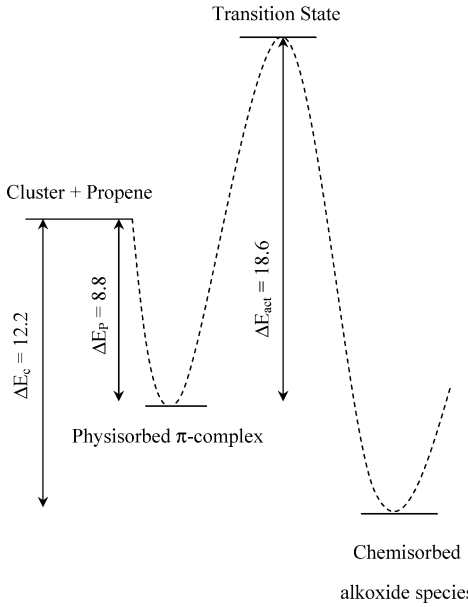

Figure 3. Energy profile for propene interaction with the Brønsted acid site depicted in Figure 2. The interaction energy of the π-complex (ΔE_p), activation energy for formation of the alkoxide species (ΔE_{act}), and enthalpy of adsorption for propene (ΔE_c) were computed to be 8.8, 18.6, and 12.2 kcal/mol, respectively.

bond with respect to the Al−O24 bond, which suggests Al−O elongation for the framework oxygen associated with alkoxide intermediates is similar in principle to elongation observed with Brønsted acid protons. The adsorption energy predicted for propene adsorption was 12.3 kcal/mol. Figure 3 shows the energy profile corresponding to the formation of the surface alkoxide from the isolated reactants.

Viruela-Martin et al.,[24] Evleth et al.,[30] and Rigby et al.[31] have also investigated the reaction mechanism and energetics associated with propene adsorption. Viruela-Martin et al.[24] evaluate the effects of isomorphous substitution for propene and isobutene adsorption using a **3T** cluster and 3-21G basis set. The physisorption interaction energy calculated by Viruela-Martin et al.[24] is similar to the value we obtain here; however, their adsorption energy and activation energy appear to be higher than our values. Comparison with an experimental study done by Aronson et al.,[22] which reports an energy profile similar to the one we predict, leads us to believe the 3T cluster is too small to accurately evaluate activation energy, yet may be suitable to obtain qualitative information. Evleth et al.[30] compute the interaction of ethylene, propene, and acetylene on **1T** and **2T** zeolite models. The activation energy they compute for propene adsorption at the MP2/6-31G* level of theory is almost identical to the value we present here. The energetics evaluated by Rigby et al.[31] on a **3T** cluster are similar to those calculated by Viruela-Martin et al.[24] Table 2 compares the energetics evaluated by Viruela-Martin et al.,[24] Evleth et al.,[30] Rigby et al., [31] and this work.

Effect of Proton Location. Experimental studies suggest that an acidic proton is not fixed to a specific framework oxygen; rather it migrates from one site to another. Variable temperature ^{1}H magic-angle spinning (MAS) NMR studies of dehydrated H-ZSM-5 provide evidence that acidic protons migrate between the four oxygen atoms surrounding the tetrahedral aluminum center.[48]

Theoretical investigations have also confirmed proton mobility in zeolites and have shown that proton mobility is greatly enhanced by trace amounts of water present in the micropores.[49,50] To investigate the effect of proton location on propene adsorption we computed geometries and energies associated for interaction of propene with the **10T** cluster (shown in Figure 1) but with the Brønsted acid proton located at O20 and subsequent secondary alkoxide formation at O24. The optimized geometries along with the associated energy profile are shown in Figure 4. The O24 site is situated right at the intersection of the sinusoidal and z-channel and represents the most accessible site for adsorption in the ZSM-5 lattice.

Analogous to the physisorbed π-complex formation for the proton located at O24, the Brønsted acid proton located at the O20 oxygen interacts with the C1−C2 double bond of propene in a similar fashion. The notable difference comparing π-complex formations is the increase in the distances between the acidic proton and the two carbons of the propene double bond C1 and C2 (from 2.10 to 2.38 Å for C1 and 2.26 Å to 2.49 Å for C2). We believe this is due to a more sterically hindered physisorbed π-complex formed on O24, and a slight decrease in the corresponding adsorption energy was expected. We computed this energy to be 7.1 kcal/mol vs 8.8 kcal/mol for the O24 proton site.

The transition state for formation of the alkoxide intermediate in the O20 proton configuration differs in comparison to the O24 proton configuration shown in Figure 2(b). The O−H bond length is 1.43 Å (compared to 1.97 Å), and the C1−H distance was 1.26 Å (compared to 1.11 Å). A Mulliken charge analysis reveals that the net charge on the $C_3H_7^+$ transition state decreases from 0.695e to 0.672e, even though the charge separation between the C1−H fragment increases due to the elongated C1−H bond distance. In keeping with the reduced charge on the transition state, the computed activation energy also decreased from 18.6 kcal/mol to 15.5 kcal/mol. No hydrogen bonding interactions were observed at the transition-state geometry in this case.

The formation of the alkoxide species in the O20 proton configuration occurs via the formation of the C2−O24 bond. The C−O bond length (1.525 Å) and the carbon−oxygen charge separation (C2 = 0.110e and O24 = −0.667e) closely resemble that observed for C2−O20 bond formation on the H−O24 configuration (C−O bond length of 1.522 Å and a carbon−oxygen charge separation of C2 = 0.109e and O20 = −0.679e). However, the energy of alkoxide formation in this case was computed to be 18.5 kcal/mol compared to 12.2 kcal/mol for C2−O20 bond formation.

Effect of T-Site. The distribution and location of framework aluminum in H-ZSM-5 has been subject to a large number of theoretical investigations.[51−54] A variety of crystallographic positions are predicted to be the most favorable for aluminum siting; however, the calculated energetic heterogeneity in the studies above is small, and hence a distribution of aluminum siting is expected. A recent experimental study by Dedecek et al.[55] also suggests that the distribution of aluminum in ZSM-5 is affected by the Si/Al composition and the synthesis procedure.

To investigate the effect of aluminum siting within ZSM-5, we computed the geometries and energies associated with the formation of the physisorbed π-complex and a chemisorbed alkoxide species for a **15T** cluster with aluminum substitution at the T4 site and Brønsted acid proton located at O17. A comparison between the T4 site (**15T**) optimized geometry shown in Figure 5(a) and the T12 site (**25T**) optimized geometry shown in Figure 1(b) reveals a longer Al−O bond length (1.89 Å relative to 1.83 Å), a wider Si−O−Al bond angle (136.40° compared to 131.04°), a wider O−Al−O bond angle (90.04° compared to 88.88°) for the T4 site, and identical O−H bond

TABLE 2: Comparison of Energetics for Propene Adsorption[a,b]

	Viruela-Martin et al.[24] (3T cluster)	Evleth et al.[30] (2T cluster)	Rigby et al.[31] (3T cluster)	this work (10T cluster)[d]	this work (25T cluster)
physisorption energy	5.9		8.4	8.8	7.1
activation energy	35.7	19.1[c]	25.0	18.6	
chemisorption energy	17.6		27.2	12.2	10.9

[a] Energy values are in kcal/mol. [b] Via secondary alkoxide formation. [c] Calculated at the MP2/6-31G* level of theory. [d] Calculated for the 10T cluster shown in Figure 1.

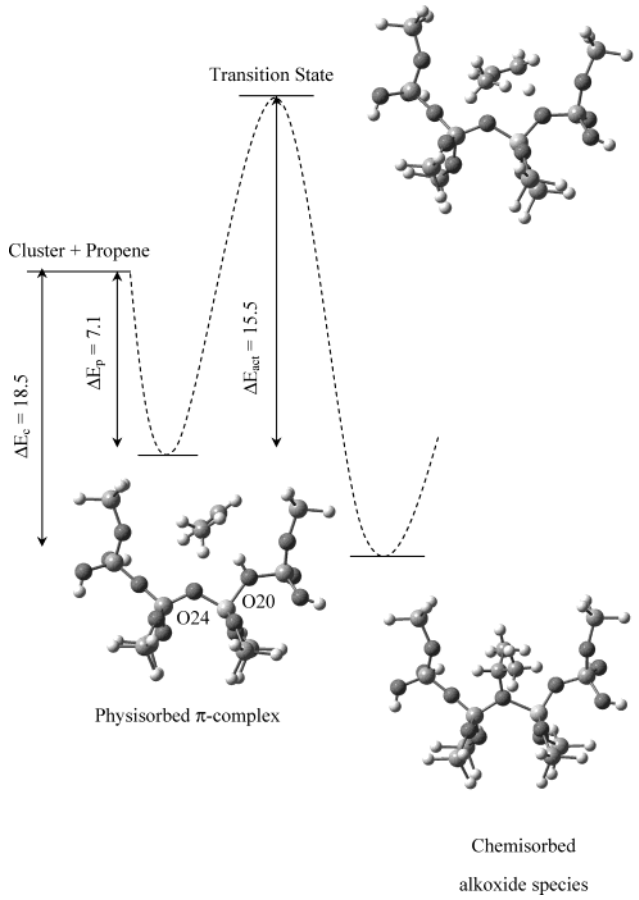

Figure 4. Optimized geometries and the associated energy profile for propene interaction with the Brønsted acid site located at O20. The interaction energy of the π-complex (ΔE_p), activation energy for formation of the alkoxide species (ΔE_{act}), and the enthalpy of adsorption of propene (ΔE_c) were computed to be 7.1, 15.5, and 18.5 kcal/mol, respectively.

lengths of 0.97 Å. The T4 site, unlike the T12 site, is accessible only via the sinusoidal channel and hence represents a distinct contrast to the T12 site.

The relaxed geometry for the physisorbed complex at the T4 site is shown in Figure 5(b). The geometrical characteristics were similar to those observed for propene physisorption described above. A slight enhancement in the O−H bond length (∼1.00 Å compared to ∼0.98 Å for the isolated cluster) was observed, while virtually no difference in the geometry of the propene molecule was observed. A Mulliken charge analysis shows an enhancement in the net charge on C1 carbon atom ≈ -0.40e (relative to −0.33e in the gas-phase molecule), similar to that observed for the physisorbed π-complex in case of the T12 site discussed in section 3.2. The formation of the physisorbed, π-complex was exothermic, and the adsorption enthalpy was calculated to be 8.1 kcal/mol.

The relaxed geometry for the corresponding alkoxide complex is shown in Figure 5(c). The resulting adsorption energy was calculated to be 7.1 kcal/mol. We note that the chemisorption energy differs significantly from the values reported for the T12 site. We attribute these differences to the more constrained environment of the T4 site, resulting in enhanced interaction of the adsorbed alkoxide intermediate with the zeolite walls. This effect is also evident from observing the C2 carbon residing a greater distance from the zeolitic oxygen (1.57 Å relative to 1.52 Å for the T12 site), resulting in the destabilization of the alkoxide species.

Primary versus Secondary Alkoxide. To investigate the relative stability of primary and secondary alkoxy intermediates and to study the dependence of activation energy on the corresponding carbenium-ion-like transition states, we computed the adsorption of propene with the **10T** cluster to form a primary alkoxide species. Two different reaction paths to the formation of the primary alkoxide species were observed. The first path involved proton transfer from O24 followed by C1−O20 alkoxide bond formation. The second path involved proton transfer from O24 followed by C1−O24 alkoxide bond formation, that is, the alkoxide species is formed on the framework oxygen that originally hosts the Brønsted acid proton. This reaction mechanism stands out in that it does not involve the bifunctional nature of the zeolite.

The optimized geometries for formation of the physisorbed π-complex, transition state, and primary alkoxide species, along with the associated energy profile resulting from the C1−O20 formation, are shown in Figure 6. The relaxed geometry for the physisorbed π-complex involves rotation of the methyl group relative to the geometry in Figure 2(a). The interaction parameters (bond lengths and bond angles) are however similar to those observed for the secondary alkoxide, and the interaction energy was computed to be 8.9 kcal/mol—almost identical to the value in section 3.2. The corresponding transition state involves significant geometrical rearrangement, and the activation energy was calculated to be 29.1 kcal/mol.

Charge distribution calculations also give more insight into the carbenium-ion-like nature of the transition state. The net charge on the transition state is 0.627e for the protonation of propene to form the 1-propoxy species on O20. This state has net lower charge relative to formation of the 2-propoxy species on O20 (0.695 e). The formation of the primary alkoxide species is slightly more exothermic compared to the secondary alkoxide species, consistent with the shorter C1−O20 bond length of 1.496 Å compared to 1.52 Å calculated for the secondary alkoxide.

The optimized geometries for formation of the π-complex, transition state, and primary alkoxide species along with the associated energy profile resulting from the C1−O24 formation are shown in Figure 7. The net charge on the transition state (0.760e) is higher for this reaction path. Analogous to the other transition-state geometries described, a significant elongation of the O−H bond, with a commensurate decrease in the C2−H bond distance, was observed. The computed activation energy was 33.9 kcal/mol, and the adsorption energy of the primary alkoxide intermediate was calculated to be 18.2 kcal/mol, which

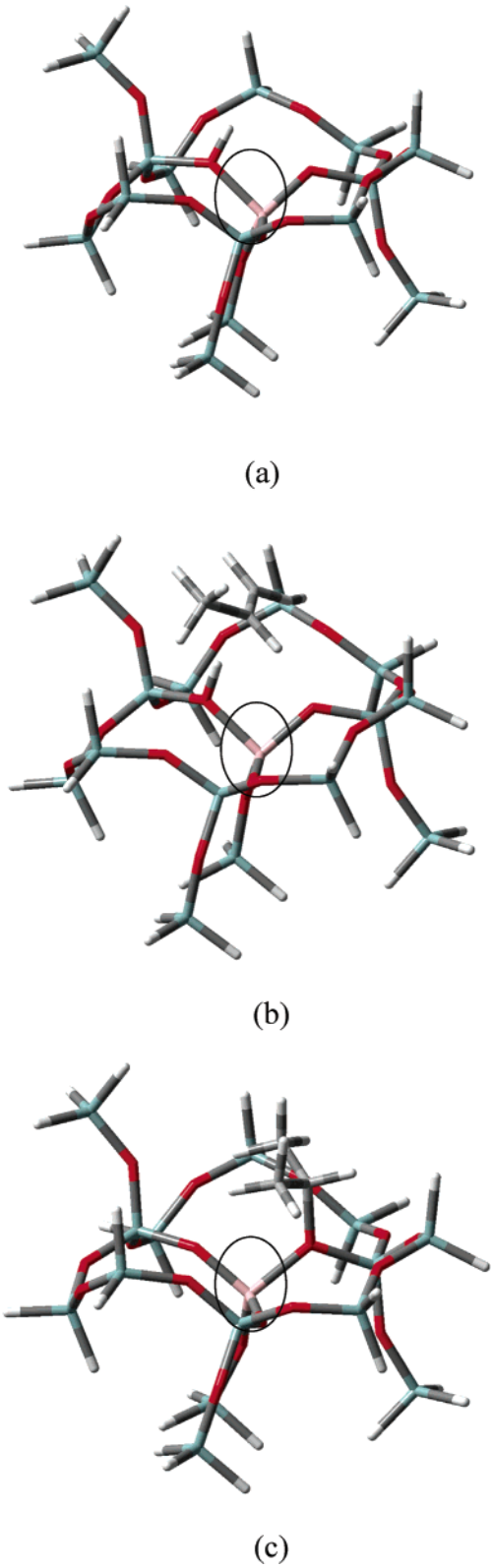

Figure 5. Optimized geometries for (a) 15T cluster with aluminum substitution at the T4 site of ZSM-5, (b) π-complex resulting from interaction of propene with the cluster in (a), and (c) the covalent secondary alkoxide species resulting from chemisorption of propene. The circle depicts the location of aluminum within each cluster.

is similar to that computed for the secondary alkoxide intermediate. Hence, contrary to what is known for carbocations in the gas phase and solution, the primary and secondary alkoxide species have comparable stability within the zeolite cavity. Also, analogous to the stability of the secondary alkoxide species,

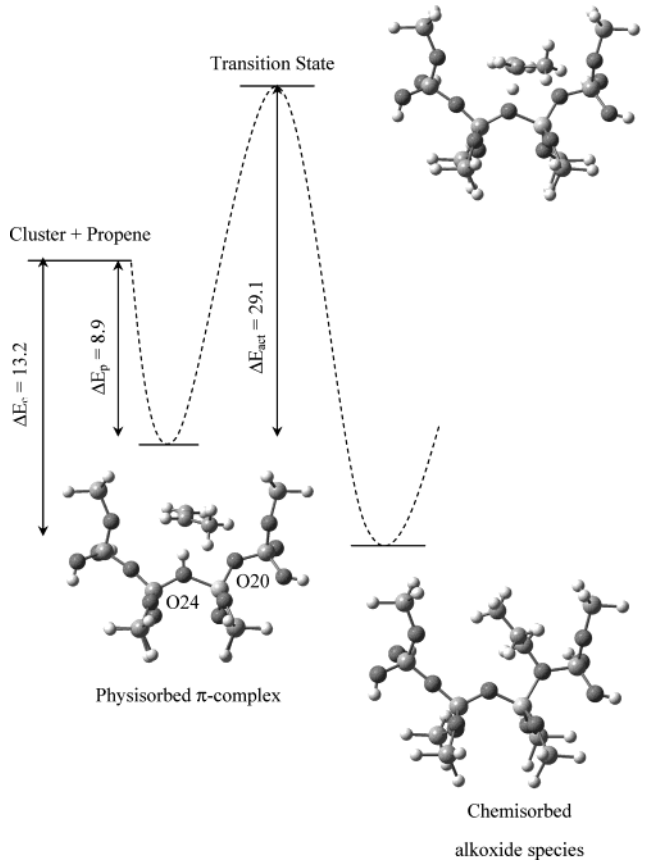

Figure 6. Optimized geometries and the associated energy profile for propene interaction with the Brønsted acid site located at O24 with alkoxide formation resulting via formation of the C1−O20 bond. The interaction energy of the π-complex (ΔE_p), activation energy for formation of the alkoxide species (ΔE_{act}), and the enthalpy of adsorption of propene (ΔE_c) were computed to be 8.9, 29.1, and 13.2 kcal/mol, respectively.

the primary alkoxide formed on O24 is significantly more stable than the alkoxide species formed on O20.

Effect of Cluster Size and Cluster Termination. To investigate the effect of cluster size on the stability of the alkoxide intermediate we computed the chemisorption energy of the propene alkoxide intermediate on **10T**, **17T**, and **25T** clusters. The **10T** and **17T** clusters are shown in Figure 8, and the **25T** cluster is shown in Figure 1(b). Terminal Si and H atoms were kept fixed in each case to provide a consistent comparison. The chemisorption energies of the secondary propene alkoxide intermediate for adsorption on the O20 site were calculated to be 8.3, 6.6, and 10.9 kcal/mol on the **10T**, **17T**, and **25T** clusters. This lack of convergence with cluster size with respect to proton affinity and interaction of ammonia has been previously observed and discussed by Brand and co-workers.[41] Unfortunately, the effects of cluster size versus degree of relaxation cannot be separated in our work, and based on the convergence trends we report, we feel that emergent methods such as QM/MM are better equipped for these types of studies.

In addition, we note that the chemisorption energy of the secondary propene alkoxide intermediate on the T12−O20 site appears to change significantly, from 12.2 kcal/mol to 8.3 kcal/mol, upon changing the cluster termination. A Mulliken charge analysis reveals that the alkoxide intermediate shown in Figure 2(c) has higher positive charge which may arise due to induction by the O−H termination, which acts as a silanol group. In addition, a greater degree of cluster relaxation was allowed in case of the O−H terminated cluster. Geometry relaxation is

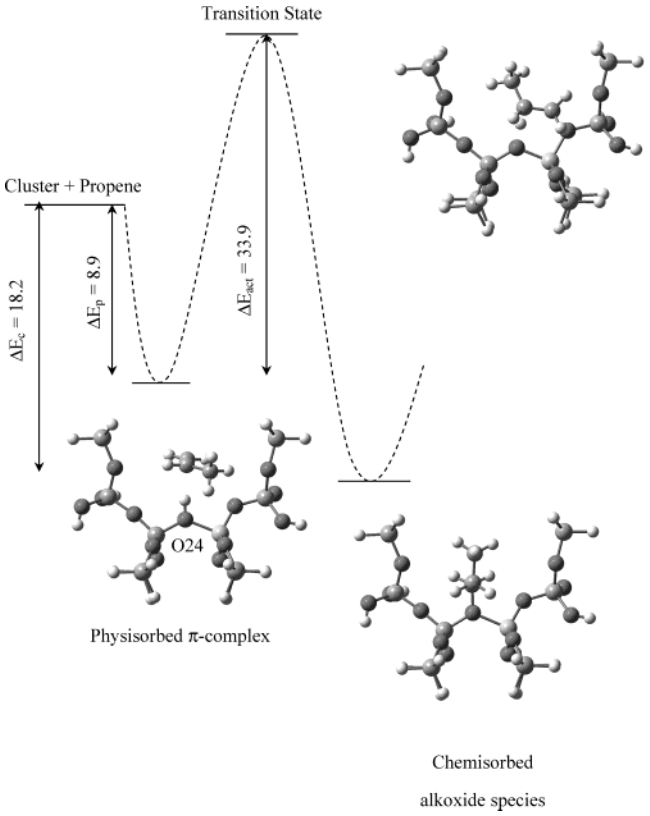

Figure 7. Optimized geometries and the associated energy profile for propene interaction with the Brønsted acid site located at O24 with alkoxide formation resulting via formation of the C1−O24 bond. The interaction energy of the π-complex (ΔE_p), activation energy for formation of the alkoxide species (ΔE_{act}), and the enthalpy of adsorption of propene (ΔE_c) were computed to be 8.9, 33.9, and 18.2 kcal/mol, respectively.

known to have a significant impact on energetics in the case of cluster studies.[41] In particular, van Santen and co-workers[38,56] found that relaxation effects significantly alter the energy of the "σ-form" alkoxide intermediate for propene chemisorption in chabazite. In all cases a greater degree of relaxation corresponded to stronger adsorption, and we report a similar observation in this case. However, as stated above, from our work it is not possible to clearly delineate relaxation versus cluster termination effects.

As stated above, we computed the energy of primary and secondary alkoxide formation on O20 and O24 for propene with the **10T** cluster described above. The energy of the secondary alkoxide intermediate is computed to be 8.3 and 12.0 kcal/mol at the O20 and O24 sites (see Figure 9(a),(b)), while the energy of the primary alkoxide intermediate is computed to be 8.4 and 12.9 kcal/mol. However, to test the effect of cluster termination, we also computed the propene chemisorption energy for the secondary alkoxide intermediate on a cluster more symmetric about the O20 site. This was intended to verify that changes in interaction energy were not a function of proximity to terminal SiH_3 groups. In comparison with the geometry shown in Figure 2(c) (in which the alkoxide is bound to the O20 site located near the outer end of the cluster rather than in the center), a new cluster more evenly distributed about the O20 site with SiH_3 termination was used for this calculation (Figure 9(c)). The chemisorption energy was observed to increase by 1.9 kcal/mol compared to 8.3 kcal/mol described above. The chemisorbed geometry at the O20 site in Figure 9(c) closely resembles that observed at the O24 site in Figure 9(a) in terms of C−O bond distance and the net charge on the alkoxide fragment.

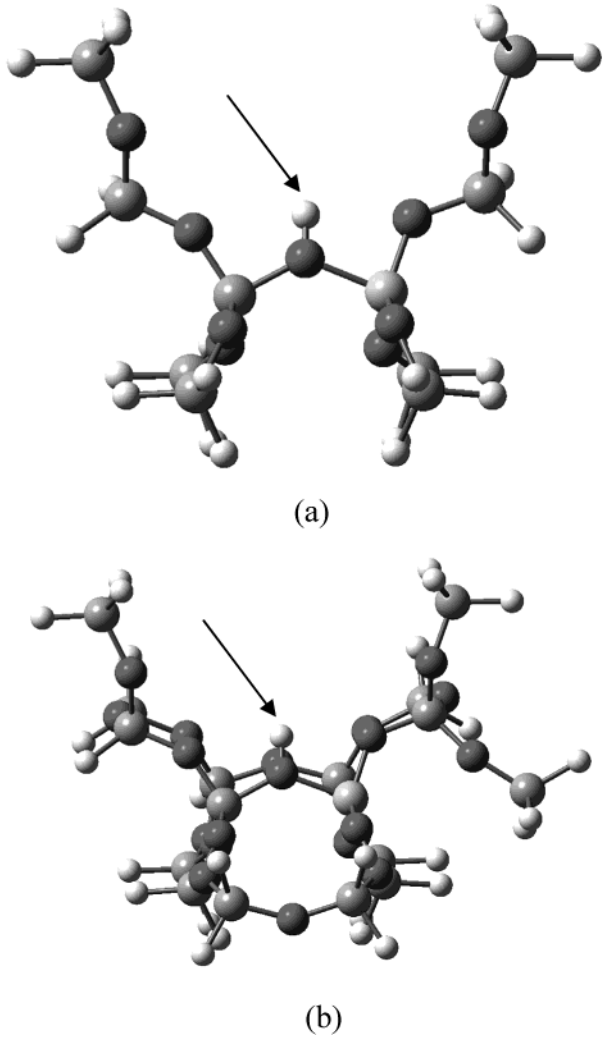

Figure 8. Structures of 10T and 17T clusters with aluminum substitution at the T12 site employed to investigate the effect of cluster size. The arrow indicates the location of the acidic proton.

Small differences with respect to the charge on the alkoxide carbon and the proximity of the hydrogen atom bonded to this alkoxide carbon to the zeolite lattice are however observed. We believe this to be a more appropriate comparison of adsorption between the O20 and O24 sites. This result suggests either different intrinsic adsorption energies for the two different oxygen lattice sites or that minute structural factors play a role in the stability of the alkoxide intermediate. We note that the interaction energies at the O24 site for the primary and secondary alkoxide intermediate also change. The primary and secondary alkoxide intermediates have comparable stability on either of the two lattice oxygen positions, and our results show that the alkoxide intermediates located on the O24 site are more stable than those located on the O20 site. This is consistent with what we expect from an assessment of pore geometry. The O24 site is located at the precise intersection of the sinusoidal and z-channel in ZSM-5, hence it is more accessible than the O20 site situated slightly off this intersection.

3.4. Hexene Adsorption. *1-Hexene Adsorption.* To investigate carbon number dependence of the energetics of olefin adsorption, we calculated the interaction of 1-hexene with the **10T** cluster (T12 Brønsted acid site with proton residing on O24). Analogous to propene, the C1−C2 double bond in 1-hexene forms a physisorbed π-complex with the Brønsted acid proton. The geometric characteristics are very similar to those

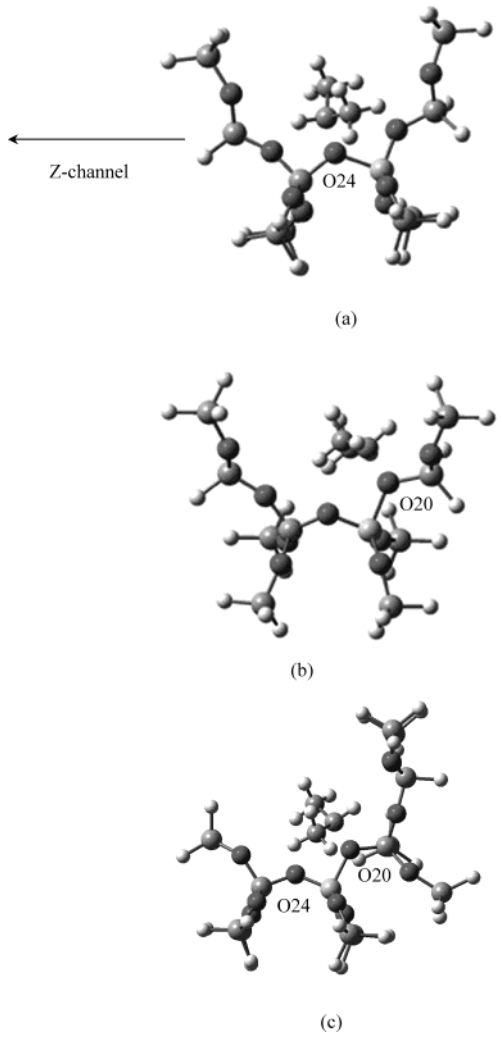

Figure 9. Optimized geometries for covalent secondary propene alkoxide intermediate with adsorption on (a) 10T cluster at the T12−O24 site, (b) 10T cluster at the T12−O20 site, and (c) 13T cluster at the T12−O20 site chosen to represent a more symmetric environment about the O20 site.

observed for propene, and the adsorption energy for physisorption was computed to be 8.3 kcal/mol.

The geometry of the transition state for formation of the alkoxide species is similar to that already described for propene on O24 and relative to the physisorbed state involves a notable increase in the O−H bond length from 0.99 to 1.76 Å and in the C1−C2 bond distance from 1.34 to 1.43 Å (a distance intermediate between a single bond and a double bond). The observed C2−O distance of 2.59 Å reinforces the viewpoint that the primary reaction coordinate involves the C2−O bond formation. We computed the activation energy to be 19.1 kcal/mol.

The formation of the alkoxide species is analogous to secondary alkoxide formation for propene described in section 3.2, with a relaxed C−O bond length of 1.52 Å and C1−C2 and C2−C3 bond lengths of 1.53 Å. The formation of the alkoxide species was computed to be exothermic by 10.4 kcal/mol. Figure 10 shows the energy profile for the interaction of 1-hexene with this Brønsted acid site.

Effect of Cluster Size on 1-Hexene Adsorption. To investigate the effect of cluster size, we calculated interaction energies of the physisorbed π-complex and alkoxide species for 1-hexene with the **25T** cluster shown in Figure 1. We observed a deviation in the O−Al−O bond angle of similar magnitude as the 10T

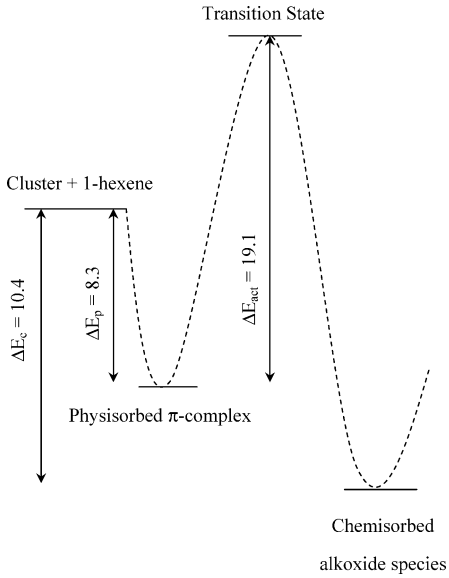

Figure 10. Energy profile for the interaction of 1-hexene with the Brønsted acid site of the 10T cluster depicted in Figure 1. The interaction energy of the π-complex (ΔE_p), activation energy for formation of the alkoxide species (ΔE_{act}), and the enthalpy of adsorption for propene (ΔE_c) were computed to be 8.3, 19.1, and 10.4 kcal/mol.

cluster (90.57° versus 95.45° in the **10T** cluster) and an increase in the equilibrium distance between the H atom of the Brønsted acid group and the C1 carbon of 1-hexene (from 2.077 to 2.136 Å). The increase in the equilibrium distance between the Brønsted acid proton and the C−C double bond of 1-hexene leads to a slight decrease in adsorption energy from 8.3 kcal/mol to 6.9 kcal/mol. The change in energy from the physisorbed state to the alkoxide increased by only ∼0.4 kcal/mol in the **25T** cluster relative to the **10T** cluster.

3-Hexene Adsorption. We investigated the effect of double bond position on olefin adsorption energetics by repeating our 1-hexene adsorption calculation on the **10T** cluster with 3-hexene. The adsorption of the physisorbed π-complex was observed to be exothermic at 9.5 kcal/mol. This slightly enhanced interaction energy relative to 1-hexene (8.3 kcal/mol) is perhaps due to the 3-hexene locating centrally within the **10T** cluster and thus may be a cluster size effect.

The transition-state geometry for formation of the alkoxide intermediate compared to the geometry of the physisorbed state was nearly identical to the 1-hexene case, the notable difference being an increase in the OH distance to 1.81 Å for the 3-hexene transition state versus 1.76 Å for the 1-hexene transition state. The formation of the transition state involved significant charge separation. The net charge on the $C_6H_{13}^+$ fragment was calculated to be 0.724e, which closely resembles a secondary carbnieum ion. The activation energy was computed to be 21.4 kcal/mol.

The formation of the alkoxide intermediate was again analogous to the primary alkoxide formation described for propene and 1-hexene. The energy of alkoxide formation, with respect to the isolated cluster and 3-hexene molecule, was computed to be 8.0 kcal/mol. The lower stabilization energy of the alkoxide species for 3-hexene (compared to 1-hexene) is probably due to steric repulsions between the substituent groups and the zeolite framework. Figure 11 shows the energy profile for adsorption of 3-hexene with this Brønsted acid site.

Effect of Cluster Size on 3-Hexene Adsorption. The energetics and geometry of 3-hexene change considerably upon interaction with the 25T cluster shown in Figure 1. The energy of formation

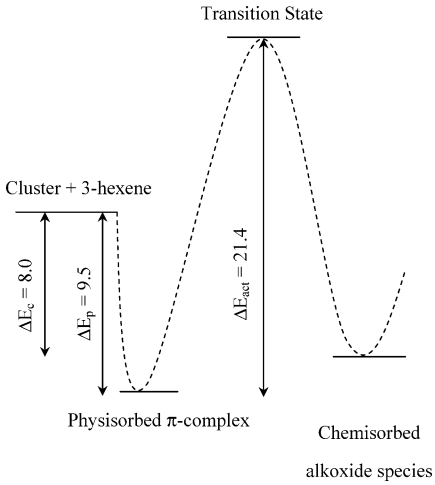

Figure 11. Energy profile for the interaction of 3-hexene with the Brønsted acid site of the 10T cluster depicted in Figure 1. The interaction energy of the π-complex (ΔE_p), activation energy for formation of the alkoxide species (ΔE_{act}), and the enthalpy of adsorption for propene (ΔE_c) were computed to be 9.5, 21.4, and 8.0 kcal/mol.

of the physisorbed π-complex was computed to be 7.7 kcal/mol, while the formation of the alkoxide species was calculated to be endothermic by 1.8 kcal/mol (with respect to the physisorbed species). Figure 12 illustrates the change in configuration of the alkoxy intermediate upon going from the **10T** to the **25T** cluster. We believe these differences are due to a more accurate representation of steric repulsions in the **25T** cluster. Boronat et al.[32] have also commented upon the greater destabilization in the alkoxide intermediate in relation to the π-complex upon imposing geometric restrictions required to simulate an active site for zeolite theta-1. We believe a similar argument can be made here.

The sensitivity of the 3-hexene alkoxide intermediate to local geometry and the effect of conformation of the alkene molecule on adsorption energetics are highlighted by comparing the energetics for the two geometries shown in Figure 13. Figure 13(b) simply represents a conformational isomer of the alkoxide intermediate shown in Figure 13(a) and described above. The formation of the alkoxide species shown in Figure 13(b), however, was determined to be exothermic by 3.4 kcal/mol (with respect to the physisorbed species).

3.5. Propane Adsorption. Calorimetric, gravimetric, and IR experiments have shown that alkanes preferentially adsorb onto Brønsted acid sites in H-ZSM-5.[15,16,57] It is known that significant nonbonding interactions exist between the adsorbate alkane molecules and the zeolite.[17] The nonbonding interactions have been shown to depend primarily on the pore diameter and fit of the alkane molecule into the pore space and to be relatively independent of the composition of the molecular sieve.[13] Derouane et al.[58] have developed an elegant model in this regard, relating the radius of curvature of the surface at the sorbing site to the strength of the interaction. However, their treatment does not account for the specific interaction between the adsorbate and the Brønsted acid site, which is one of the goals of our study.

The relaxed geometry for physisorbed propane on the Brønsted acid site of the **10T** cluster is shown in Figure 14. Localized adsorption between the apolar alkane and the zeolite occurs due to induced dipole−dipole interactions. Propane interacts weakly with the acidic proton with H−H distances of about 2.15 Å, and the adsorption energy was computed to be 2.7 kcal/mol. To determine the contribution of acid sites to the heat of adsorption, Eder et al.[15,16] measured the sorption enthalpy

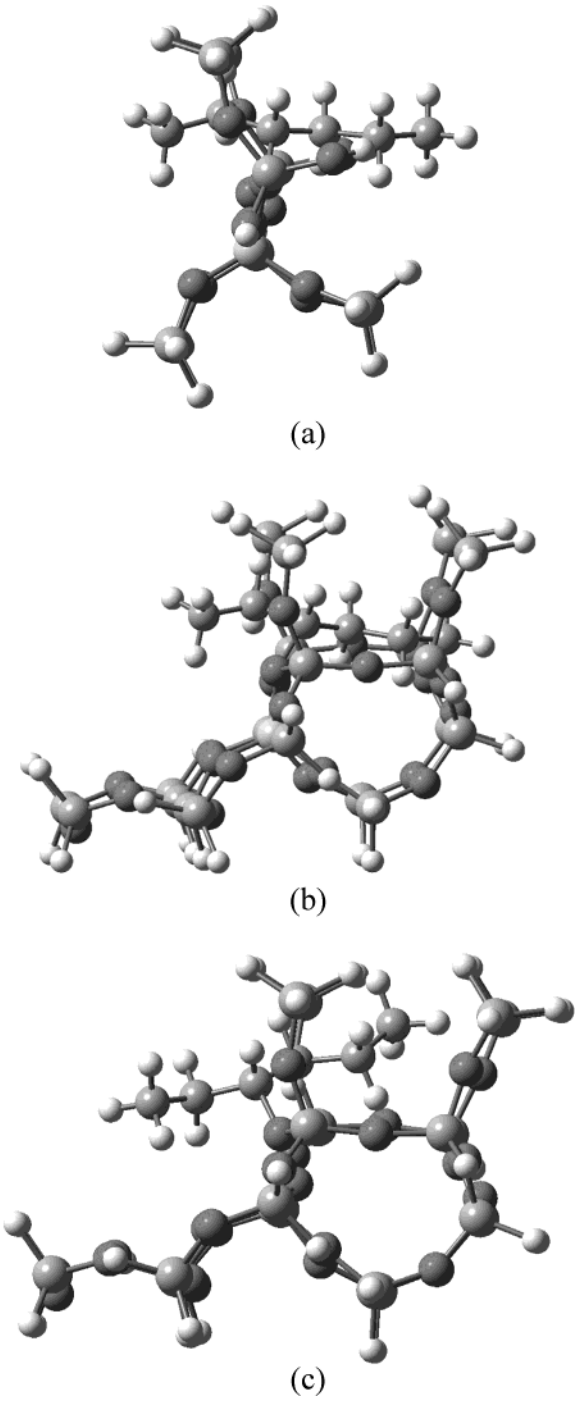

Figure 12. Effect of cluster size on the alkoxide geometry for 3-hexene: (a) optimized geometry for alkoxide formation in 10T cluster, (b) the optimized geometry in (a) with 25T cluster from Figure 1 superimposed, and (c) optimized geometry for alkoxide intermediate in the 25T cluster.

on purely siliceous and acidic samples of the MFI structure. The acidic and siliceous samples were found to exhibit a constant 10 kJ/mol (2.4 kcal/mol) difference independent of the carbon number of the alkane adsorbed. Our theoretical predictions for the alkane-acid site interaction in MFI compare favorably with experimental results.

4. Discussion

Our DFT calculations demonstrate that the stability of the covalent alkoxide intermediates formed upon olefin adsorption depend to an extent on the interaction of the protonated molecule

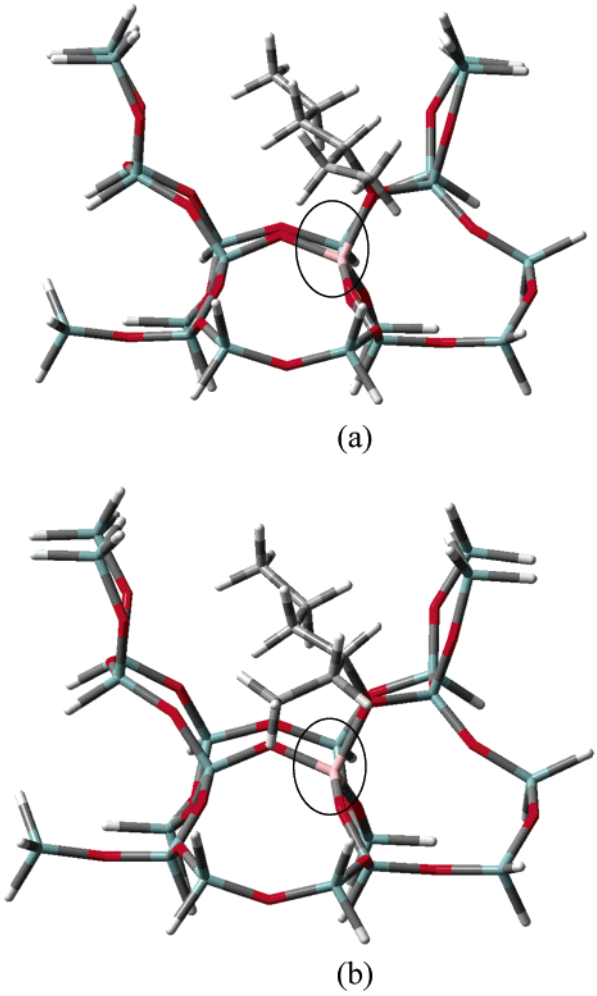

Figure 13. Effect of olefin conformation and interactions with the zeolite walls on the alkoxide stability for 3-hexene: (a) optimized geometry for alkoxide intermediate in 25T cluster, the alkoxide formation was computed to be endothermic by 1.8 kcal/mol and (b) optimized geometry for alkoxide intermediate in 25T cluster, the alkoxide formation was computed to be exothermic by 3.4 kcal/mol. The circle depicts the location of aluminum in each cluster.

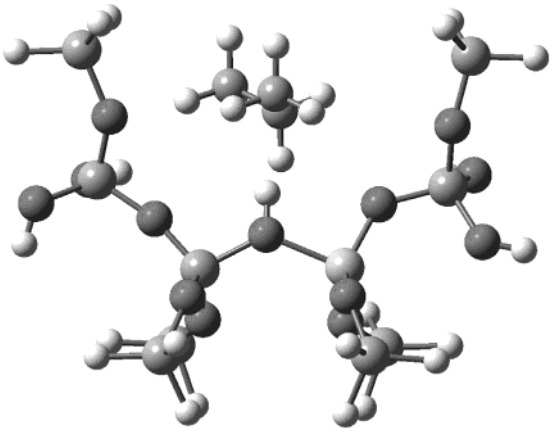

Figure 14. Optimized geometry for interaction of propane with the Brønsted acid site of the 10T cluster depicted in Figure 1. The specific interaction was computed to be 2.7 kcal/mol.

with the neighboring zeolite wall. This is clearly illustrated by three observations reported here.

The first observation relates to the significant increase in the energy of alkoxide formation for propene upon proton placement at O24 vs O20. For each of the two sites identical C−O bond distances are calculated: 1.49 Å for the primary and 1.52 Å for the secondary alkoxide species. Hence, we conclude that the resultant energy differences are not due to different C−O bond energies. The aforementioned values were computed relative to the isolated zeolite cluster and the propene molecule, and the isolated clusters in themselves differ by only ∼0.25 kcal/mol. By inspection we see that the O20 site is near the wall; however, the O24 site is located closer the center of the zeolite cavity. Thus despite the similarity in the C−O bonding, the 6 kcal/mol difference in adsorption energy is best accounted for by the proximity to the zeolite wall of the resulting alkoxide species. A similar observation with respect to the primary alkoxide species described in section 3.3 reaffirms this idea. This observation is consistent across O−H or Si−H termination, as described in section 3.3.

The second observation is the different energy values computed for propene adsorption at the T12 and T4 sites. We note that the difference between the interaction energies for the propoxide intermediate computed for the T12−O24 (**10T**) and T4−O17 (**15T**) site is greater than the difference between the T12 site computed for the **10T** and **25T** cluster sizes and, hence, is not an effect of cluster size.

The third observation concerns the very different values computed for different conformational isomers of the alkoxide intermediate for 3-hexene. The fact that the stability of the alkoxide intermediate is so sensitive to the local geometry of the active site and interactions with the zeolite wall implies a wide distribution of olefin protonation energies within the zeolite and calls attention to the need to account for local site geometry in comparing reactivity of different zeolite structures. Boronat et al.[32] come to a similar conclusion based on their theoretical investigation of olefin adsorption on the unidimensional theta-1 zeolite. The above discussion emphasizes the nonuniformity of sites in zeolites associated with isolated framework aluminum substitution in nonequivalent crystallographic sites. Recent periodic DFT calculations by Rozanska et al.[39] also comment upon the destabilization of the chemisorbed alkoxy species due to steric constraints. Although our results on the effects of cluster size and termination effects do not demonstrate convergence, we observe that the trends observed in the stability of primary and secondary alkoxide intermediates do not depend on the cluster termination even though the absolute energies are sensitive to cluster termination as well as to the degree of relaxation of the cluster employed.

A comparison of propene, 1-hexene, and 3-hexene to form secondary alkoxide species on O24 reveals that the stability of the alkoxide intermediates does not depend significantly on the carbon number. Further, the stability of the alkoxide species does not follow the order of stability observed for carbocationic species in the solution phase as is evident upon comparing the energies of adsorption of the primary and secondary propoxide species on the O20 and O24 sites. Therefore, differences between the hydrocarbon conversion reaction rates in zeolites can be ascribed to the transition state and not the ground-state alkoxide intermediates. The transition states have significant ionic character, and our observed activation barriers for formation of the primary and secondary propoxide species are consistent with the carbenium-ion-like character of the transition state. The success of carbenium ion models for predictions of preferred reaction pathways in zeolites has been attributed to an ordering of activation barriers rather than the relative stabilities of the intermediates in the literature.[25,31,59] In addition, we show that the activation barrier does not reflect any carbon number dependence, which appears contrary to the notion that

longer chain alkenes, with more electron donating groups, should stabilize the carbenium-ion-like transition state by lowering its charge. But, we believe that this increase in number of electron-donating methylene groups is counteracted by the increased steric hindrance of the corresponding transition state. This results in the bulkier transition state being situated further away from the zeolite walls, which reduces the stabilizing effect of the negatively charged zeolite wall on the positively charged transition state. The covalent surface alkoxide species also do not appear to be as stable as some early theoretical studies have suggested (see Table 2 and references therein) and, therefore, may be reactive for several zeolite-catalyzed reactions such as hydride transfer, alkylation, β-scission, etc.

In addition, this work confirms other theoretical investigations[33,34] that report coordination between the protonated transition state and all three available oxygens surrounding the aluminum site during the proton transfer. Although we are unable to quantify the magnitude of this interaction, we believe that this nucleophillic interaction has a tendency to stabilize the positively charged transition state and, hence, may be central for activation energy calculations. In this context we would like to highlight the importance of cluster size used to model the acid site. Recent theoretical calculations on MOR, TON, and CHA by Rozanska et al.[39] also correlate the activation energy for isobutene protonation with the number of framework oxygen atoms that coordinate with the carbenium-ion-like transition state and zeolite micropore dimension.

Several researchers have previously commented upon the need to consider Brønsted acidic centers in conjunction with the neighboring basic sites, that is, with the negatively charged oxygen atoms of the zeolite, bonded to the aluminum atoms.[1,6,24,25] A bifunctional mechanism for olefin adsorption, with the acid moiety acting as a proton donor and the basic moiety stabilizing the protonated species, has been postulated to be the reaction pathway in this work as well as several other theoretical investigations. However, in section 3.3 we demonstrate, for the first time, the protonation of a propene molecule to form a primary alkoxide species bonded to the original host oxygen of the acidic proton. The activation energy calculated for this pathway (33.9 kcal/mol) is comparable to that evaluated for the bifunctional pathway (29.1 kcal/mol), and hence we postulate this pathway to be feasible.

The adsorption energetics for large molecules such as hexene within H-ZSM-5 has continued to remain elusive due to the large cluster sizes, and hence computational resources, required. However, it forms a critical part in, for example, our current efforts to understand the elementary steps for cyclization and aromatization within the zeolite cavity.[60] We report here that the energy of formation of the π-complex is relatively independent of the position of the double bond in hexene, while the alkoxide stability is sensitive to the local zeolite site geometry and adsorbate conformation.

Sorption phenomena have been sited as the primary reason for enhancement in unimolecular activation of paraffins with increasing carbon number in H-ZSM-5. Hence, the adsorption process is important in the investigation of the barriers for proton cracking and transfer. Although the treatment of correlation in density functional theory has been questioned for calculating weak interaction energies,[61] we report here energies for specific interaction of propane with the Brønsted acid site that agree well with measured experimental values.

5. Conclusion

In summary, we conclude that the protonation energy of an olefinic molecule is relatively independent of carbon number but varies significantly with the extent of interaction with the zeolite wall and steric hindrance. Hence, the protonation energy of a molecule not only is indicative of the interaction between the Brønsted acid proton and the molecule but also depends to a significant extent on the interaction of the protonated molecule with the zeolite wall. Thus, changes in zeolite structure may affect the energetics of alkoxide formation dramatically. We evaluated the activation barrier for alkoxide formation to be independent of carbon number and a function of the nature (primary vs secondary) of the carbenium-ion-like transition state. We also observe coordination between multiple oxygens attached to the aluminum center at the transition-state geometry. Our calculations also provide evidence for an olefin protonation mechanism that does not involve the bifunctional (acid−base) nature of the zeolite with an activation energy that is comparable to bifunctional mechanisms calculated by us and other groups.

Acknowledgment. The Indiana 21st Century Research and Technology Fund supported this work. Computational support was provided by a grant from the National Computational Science Alliance (NCSA Grant ESC030001) and the Purdue University Computing Center (PUCC).

References and Notes

(1) Kazansky, V. B.; Senchenya, I. N. *J. Catal.* **1989**, *119*, 108.
(2) Kramer, G. J.; van Santen, R. A.; Emeis, C. A.; Nowak, A. K. *Nature* **1993**, *363*, 529.
(3) Sauer, J. *Nature* **1993**, *363*, 493.
(4) van Santen, R. A. *J. Mol. Catal. A: Chem.* **1997**, *115*, 405.
(5) van Santen, R. A. *Catal. Today* **1997**, *38*, 377.
(6) Kazansky, V. B. *Catal. Today* **1999**, *51*, 419.
(7) van Santen, R. A.; Kramer, G. M. *Chem. Rev.* **1995**, *95*, 637.
(8) Frash, M. V.; van Santen, R. A. *Top. Catal.* **1999**, *9*, 191.
(9) Kazansky, V. B.; Frash, M. V.; van Santen, R. A. *Catal. Lett.* **1997**, *48*, 61.
(10) Boronat, M.; Viruela, P.; Corma, A. *J. Phys. Chem. B* **1999**, *103*, 7809.
(11) Frash, M. V.; Kazansky, V. B.; Rigby, A. M.; van Santen, R. A. *J. Phys. Chem. B* **1998**, *102*, 2232.
(12) Kazansky, V. B. *Stud. Surf. Sci. Catal.* **1994**, *85*, 251.
(13) Eder, F.; Lercher, J. A. *J. Phys. Chem.* **1996**, *100*, 16460.
(14) Eder, F.; Lercher, J. A. *J. Phys. Chem. B* **1997**, *101*, 1273.
(15) Eder, F.; Lercher, J. A. *Zeolites* **1997**, *18*, 75.
(16) Eder, F.; Stockenhuber, M.; Lercher, J. A. *J. Phys. Chem. B* **1997**, *101*, 5414.
(17) Savitz, S.; Siperstein, F.; Gorte, R. J.; Myers, A. L. *J. Phys. Chem. B* **1998**, *102*, 6865.
(18) Grillet, Y.; Llewellyn, P. L.; Reichert, H.; Coulomb, J. P.; Pellenq, N.; Rouquerol, J. *Stud. Surf. Sci. Catal.* **1994**, *87*, 525.
(19) Stach, H.; Lohse, U.; Thamm, H.; Schrimer, W. *Zeolites* **1986**, *6*, 74.
(20) Grady, M. C.; Gorte, R. J. *J. Phys. Chem.* **1985**, *89*, 1305.
(21) Haw, J. F.; Richardson, B. R.; Oshiro, B. R.; Lazo, N. D.; Speed, J. A. *J. Am. Chem. Soc.* **1989**, *111*, 2052.
(22) Aronson, M. T.; Gorte, R. J.; Farneth, W. E.; White, D. *J. Am. Chem. Soc.* **1989**, *111*, 840.
(23) Kondo, J. N.; Wakabayashi, F.; Domen, K. *Catal. Lett.* **1998**, *53*, 215.
(24) Viruela-Martin, P.; Zichovich-Wilson, C. M.; Corma, A. *J. Phys. Chem.* **1993**, *97*, 13713.
(25) Rigby, A. M.; Kramer, G. J.; van Santen, R. A. *J. Catal.* **1997**, *170*, 1.
(26) Zygmunt, S. A.; Mueller, R. M.; Curtiss, L. A.; Iton, L. E. *J. Mol. Struct. (THEOCHEM)* **1998**, *430*, 9.
(27) Becke, A. D. *J. Chem. Phys.* **1993**, *98*, 5648.
(28) Peng, C.; Schlegel, H. B. *Isr. J. Chem.* **1993**, *33*, 449.
(29) Frish, M. J.; Trucks, G. W.; Schlegel, H. B.; Scuseria, G. E.; Robb, M. A.; Cheesman, J. R.; Zakrzewski, V. G.; Mongomery, J. A. J.; Stratmann, R. E.; Burant, J. C.; Dapprich, D.; Millam, J. M.; Daniels, A. D.; Kudin, K. N.; Strain, M. C.; Farkas, O.; Tomasi, J.; Barone, V.; Cossi, M.; Cammi, R.; Mennucci, B.; Pomelli, C.; Adamo, C.; Clifford, S.; Ochterski, J.; Petersson, G. A.; Ayala, P. Y.; Cui, Q.; Morokuma, K.; Malick, D. K.; Radbuck, A. D.; Raghavachari, K.; Foresman, J. B.; Ciolowski, J.; Ortiz, J. V.; Baboul, A. G.; Stefanov, B. B.; Liu, G.; Liashenko, A.; Piskorz, P.; Komaromi, I.; Gomperts, R.; Martin, R. L.; Fox, D. J.; Keith, T.; Al-Laham, M. A.; Peng, C. Y.; Nanayakkara, A.; Gonzalez, C.; Challacombe, M.; Gill,

P. M. W.; Johnson, B. G.; Chen, W.; Wong, M. W.; Andres, J. L.; Head-Gordon, M.; Replogle, E. S.; Pople, J. A. Gaussian98; Revision A.9 ed.; Gaussian, Inc.: Pittsburgh, PA, 1998.

(30) Evleth, E. M.; Kassab, E.; Jessri, H.; Allavena, M.; Montero, L.; Sierra, L. R. *J. Phys. Chem.* **1996**, *100*, 11368.

(31) Rigby, A. M.; Frash, M. V. *J. Mol. Catal. A: Chem.* **1997**, *126*, 61.

(32) Boronat, M.; Zicovich-Wilson, C. M.; Viruela, P.; Corma, A. *J. Phys. Chem. B* **2001**, *105*, 11169.

(33) Correa, R. J.; Mota, C. J. A. *Phys. Chem. Chem. Phys.* **2002**, *4*, 375.

(34) Zygmunt, S. A.; Curtiss, L. A.; Zapol, P.; Iton, L. E. *J. Phys. Chem. B* **2000**, *104*, 1944.

(35) Brandle, M.; Sauer, J. *J. Am. Chem. Soc.* **1998**, *120*, 1556.

(36) Sauer, J.; Sierka, M. *J. Comput. Chem.* **2000**, *21*, 1470.

(37) Shah, R.; Payne, M. C.; Gale, J. D. *Int. J. Quantum Chem.* **1997**, *61*, 393.

(38) Sinclair, P. E.; Vries, A. d.; Sherwood, P.; Catlow, C. R. A.; van Santen, R. A. *J. Chem. Soc., Faraday Trans.* **1998**, *94*, 3401.

(39) Rozanska, X.; van Santen, R. A.; Demuth, T.; Hutschka, F.; Hafner, J. *J. Phys. Chem. B* **2003**, *107*, 1309.

(40) van Koningsveld, H.; van Bekkum, H.; Jansen, J. C. *Acta Crystallogr., Sect. B: Struct. Sci*. **1987**, 127.

(41) Brand, H. V.; Curtiss, L. A.; Iton, L. E. *J. Phys. Chem.* **1992**, *96*, 7725.

(42) Brand, H. V.; Curtiss, L. A.; Iton, L. E. *J. Phys. Chem.* **1993**, *97*, 12773.

(43) Cook, S. J.; Chakraborty, A. K.; Bell, A. T.; Theodorou, D. N. *J. Phys. Chem.* **1993**, *97*, 6679.

(44) Zicovich-Wilson, C. M.; Corma, A.; Viruela, P. *J. Phys. Chem.* **1994**, *98*, 10863.

(45) Corma, A. *Stud. Surf. Sci. Catal.* **1995**, *94*, 737.

(46) Corma, A.; Garcia, H.; Sastre, G.; Viruela, P. *J. Phys. Chem. B* **1997**, *101*, 4575.

(47) Spoto, G.; Bordiga, S.; Ricchiardi, G.; Scarano, D.; Zecchina, A.; Borello, E. *J. Chem. Soc., Faraday Trans.* **1994**, *90*, 2827.

(48) Baba, T.; Komatsu, N.; Ono, Y.; Sugisawa, H. *J. Phys. Chem. B* **1998**, *102*, 804.

(49) Ryder, J. A.; Chakraborty, A.; Bell, A. T. *J. Phys. Chem. B* **2000**, *104*, 6998.

(50) Franke, M. E.; Sierka, M.; Simon, U.; Sauer, J. *Phys. Chem. Chem. Phys.* **2002**, *4*, 5207.

(51) Alvarado-Swaisgood, A. E.; Barr, M. K.; Hay, P. J.; Redondo, A. *J. Phys. Chem.* **1991**, *95*, 10031.

(52) Redondo, A.; Hay, P. J. *J. Phys. Chem.* **1993**, *97*, 11754.

(53) Lonsinger, S. R.; Chakraborty, A.; Theodorou, D. N.; Bell, A. T. *Catal. Lett.* **1991**, *11*, 209.

(54) Grau-Crespo, R.; Peralta, A. G.; Ruiz-Salvador, A. R.; Gomez, A.; Lopez-Cordero, L. *Phys. Chem. Chem. Phys.* **2000**, *2*, 5716.

(55) Dedecek, J.; Kaucky, D.; Wichterlova, B. *Chem. Commun.* **2001**, 970.

(56) Rozanska, X.; Demuth, T.; Hutschka, F.; Hafner, J.; van Santen, R. A. *J. Phys. Chem. B* **2002**, *106*, 3248.

(57) Eder, F.; Stockenhuber, M.; Lercher, J. A. *Stud. Surf. Sci. Catal.* **1995**, *97*, 495.

(58) Derouane, E. G. *Chem. Phys. Lett.* **1987**, *142*, 200.

(59) Natal-Santiago, M. A., R.; Dumesic, J. A. *J. Catal.* **1999**, *181*, 124.

(60) Joshi, Y. V.; Bhan, A.; Thomson, K. T., submitted for publication.

(61) Curtiss, L. A.; Zygmunt, S. A.; Iton, L. E. *Ab inito and density functional studies of hydrocarbon adsorption in zeolites*, Proceedings of the International Zeolite Conference, 12th, Baltimore, 1998.